The 40^{th} International Workshop on Water Waves and Floating Bodies, 11-14 May 2025, Shanghai, China

Wave interaction and turbulent dissipation of a highly-porous periodic breakwater

Elias J. G. Arcondoulis[‡*] **& Richard Porter**[†]

[‡]School of Civil Aerospace & Design Engineering, University of Bristol, Bristol, BS8 1TR, UK
[*]Australian Maritime College, Newnham, 7248, Tasmania, Australia
[†]School of Mathematics, University of Bristol, Bristol, BS8 1UG, UK

Email: elias.arcondoulis@bristol.ac.uk

1 Introduction

Climate change is causing more frequent and intense storms that will continue to impact coastal communities. Porous breakwaters have been investigated as an alternative to solid breakwaters to minimise erosion and damage to coastline infrastructure, while permitting natural longshore drift processes. In order to model the wave attenuation of a porous breakwater, a bulk porous medium is usually modelled, yet it is unclear when the scale of the porous material influences local surface wave dynamics and vorticity under the surface and therefore the reflection, transmission and absorption coefficients of the structure. Here we investigate a highly-porous periodic breakwater presented in Fig. 1, inspired by a cylindrical porous coating study to alleviate vortex shedding by Arcondoulis *et al* (2023). A solid rectangular block with cylinder and square sections are subtracted along the y-and z-axis, and the x-axis, respectively, to create pores with comparable dimensions to wave amplitudes at higher wavenumbers achievable in a wave flume.

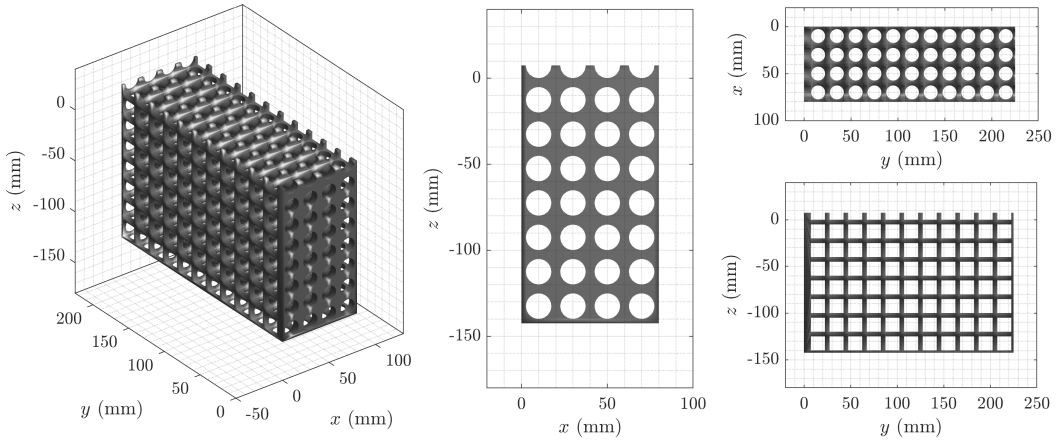

Figure 1: CAD images of an xz-plane slice of the periodic breakwater with 78% porosity.

We adopt the model developed by Sollitt & Cross (1972) to provide the governing equations and boundary conditions. Their model is carefully constructed to provide a simplified linearised description of the flow in terms of fundamental physical parameters and applies to flow in a porous medium. A series of experiments were conducted in a wave flume using (i) wave gauges to determine the reflection, transmission and absorption coefficients of the breakwater, (ii) water surface photographs to record wave diffraction and (iii) time-resolved 3-D Particle Image Velocimetry (PIV) at $z \leq -60$ mm to observe turbulent dissipation at the breakwater walls.

2 Mathematical theory

Cartesian coordinates (x, z) are chosen with z directed upwards from the rest position of the free surface of a fluid of depth d. We consider a surface-piercing breakwater structure occupying $|x| < a$ and $-b < z < 0$. Waves of angular frequency ω are normally-incident on the breakwater from $x = -\infty$ and are partially reflected and transmitted.

In the fluid region, there exists a velocity potential ϕ satisfying

$$\nabla^2\phi = 0 \tag{1}$$

with

$$\phi_z = 0, \qquad \text{on } z = -d, \tag{2}$$

$$\phi_z - K\phi = 0, \qquad \text{on } z = 0,\ |x| > a \tag{3}$$

where $K = \omega^2/g$ and g represents acceleration due to gravity. Within the porous medium the flow can also be represented by a velocity potential satisfying (1). The effect of the porous medium is manifested in a modification to the classical Bernoulli's equation. Thus, following Sollitt & Cross (1972) the surface condition representing the combined kinematic and dynamic boundary condition turns out to be expressed as

$$\phi_z - K(S + \mathrm{i}f)\phi = 0, \qquad \text{on } z = 0,\ |x| < a. \tag{4}$$

Here, $S = 1 + (1-\epsilon)C_M/\epsilon$ in terms of an added inertia coefficient, C_M, and the porosity, ϵ; f is a damping parameter which must be determined iteratively by (12). Conditions matching the fluid pressures and normal fluxes across the three submerged surfaces of the rectangular breakwater also apply. Referring to Sollitt & Cross (1972) these are given by

$$\phi(x,-b^-) = (S+\mathrm{i}f)\phi(x,-b^+), \quad \phi_x(x,-b^-) = \epsilon\phi_x(x,-b^+), \qquad \text{for } |x| < a, \tag{5}$$

$$\phi(\mp a^\mp, z) = (S+\mathrm{i}f)\phi(\mp a^\pm, z), \quad \phi_x(\mp a^\mp, z) = \epsilon\phi_x(\mp a^\pm, z), \qquad \text{for } -b < z < 0. \tag{6}$$

It remains to specify conditions at infinity and so we write

$$\phi(x,z) \sim \begin{cases} (\mathrm{e}^{\mathrm{i}kx} + R\mathrm{e}^{-\mathrm{i}kx})\psi_0(z), & x \to -\infty \\ T\mathrm{e}^{\mathrm{i}kx}\psi_0(z), & x \to \infty \end{cases} \tag{7}$$

where R and T are reflection and transmission coefficients, to be found. In (7) k is the real positive root of the dispersion relation $k\tanh kd = K$ and $\psi_0(z)$ is the depth function associated with propagating waves defined by $\psi_0(z) = N_0^{-1/2}\cosh k(z+d)$; $N_0 = \frac{1}{2}(1 + \sinh(2kd)/2kd)$ is a normalising factor. The coefficient of absorption is defined to be $\eta = 1 - \left(|R|^2 + |T|^2\right)$.

The mathematical solution involves first decomposing the problem into symmetric and antisymmetric potentials, thus

$$\phi(x,z) = \tfrac{1}{2}(\phi^s(x,z) + \phi^a(x,z)) \tag{8}$$

such that $\phi^s(x,z) = \phi^s(-x,z)$, $\phi^a(x,z) = -\phi^a(-x,z)$ are defined in $-\infty < x < 0$ with $\phi^s_x(0,z) = \phi^a(0,z) = 0$. Potentials in $x < -a$ are expressed in terms of expansions involving the standard water wave depth eigenfunctions $\{\psi_m(z), m = 0,1,\ldots\}$, but in $-a < x < 0$ we write

$$\phi^{s,a}(x,z) = \sum_{n=0}^{\infty} b_n^{s,a} \left\{ \begin{array}{c} \cos\kappa_n x \\ \sin\kappa_n x \end{array} \right\} Z_n(z) \tag{9}$$

where the upper/lower braced entries correspond to s, a (respectively). In (9), κ_n are the roots of the dispersion relation

$$\kappa_n \frac{[\epsilon\tanh\kappa_n b + (S+\mathrm{i}f)\tanh\kappa_n(d-b)]}{[\epsilon + (S+\mathrm{i}f)\tanh\kappa_n b\tanh\kappa_n(d-b)]} = K(S+\mathrm{i}f) \tag{10}$$

lying in the upper-half complex plane and ordered with increasing size of the imaginary parts which is derived alongside the piecewise definition

$$Z_n(z) = \begin{cases} \cosh\kappa_n z + (K/\kappa_n)(S+\mathrm{i}f)\sinh\kappa_n z, & -b < z < 0, \\ (S+\mathrm{i}f)\dfrac{(\cosh\kappa_n b - (K/\kappa_n)(S+\mathrm{i}f)\sinh\kappa_n b)}{\cosh\kappa_n(d-b)}\cosh\kappa_n(z+d), & -d < z < -b, \end{cases} \tag{11}$$

which accounts for the conditions (3), (4) and (5). Potentials and their derivatives are matched across $x = -a$ using (6) plus continuity of ϕ and ϕ_x across the fluid-fluid interface $x = -a$, $-d < z < -b$. Both sides of the resulting equations are multiplied by $\psi_m(z)$ $m = 0, 1, \ldots$ and integrated over $-d < z < 0$ allowing each symmetric and antisymmetric problem to be reduced to an infinite system of equations for the coefficients $b_n^{s,a}$ in (9) who values are subsequently approximated by truncation. Approximations to $|R|$, $|T|$ and η follow.

The value of f is determined iteratively from the requirement (Sollitt & Cross (1972)) that

$$f\omega = \frac{\epsilon\nu}{K_p} + \frac{8}{3\pi}\frac{\epsilon^2 C_f}{K_p^{1/2}}\left(\int_{-b}^{0}\int_{-a}^{a}|\nabla\phi|^3 dxdz\right) \Big/ \left(\int_{-b}^{0}\int_{-a}^{a}|\nabla\phi|^2 dxdz\right) \tag{12}$$

which follows from the linearisation of a turbulent drag term under the Lorentz principle of equivalent work. In (12) ν is fluid viscosity K_p is permeability, C_f is a coefficient of turbulent drag; f also depends on the incident wave amplitude, A.

3 Experiments and comparison with theory

Experiments were conducted in a 600 mm-wide wave flume in the COAST Laboratory at The University of Plymouth. The mean water depth was $d = 300$ mm, and wave gauges were placed at $x = 500$ mm and 300 mm to estimate $|R|$, and at $x = 1600$ mm and -1200 mm to estimate $|T|$, where the upstream face is at $x = 0$ mm. Thirty equispaced wavenumbers were investigated from $kd \approx 0.75$ to 3.5 and the wave amplitude was set to $2A/\lambda \leq 0.05$.

We have not attempted to experimentally measure values of the parameters in (12), instead choosing to sample parameters to determine if a fit to $|R|$, $|T|$ and η can be manufactured. In illustrative results shown in Fig. 2 we have used $a/d = 0.13$, $b/d = 0.46$, $\epsilon = 0.75$, $S = 1.6$ and $\nu g^{1/2}d^{1/2}/K_p = 0.001$, $8AgdC_f/(3\pi K_p^{1/2}\psi_0(0)) = 0.03$. Although general trends are captured at lower kd-values, the present theory is not able to reproduce experimental results beyond $kd \approx 2.8$. A possible explanation is that the Sollitt & Cross (1972) porous medium theory is not appropriate for the periodic structured breakwater design. Instead, we believe that an adaptation of the theory of Mei *et al* (2014), designed for turbulent dissipation in periodic structures, would give better agreement. This approach requires greater theoretical effort including CFD simulations in fundamental cells and experimental parameterisation.

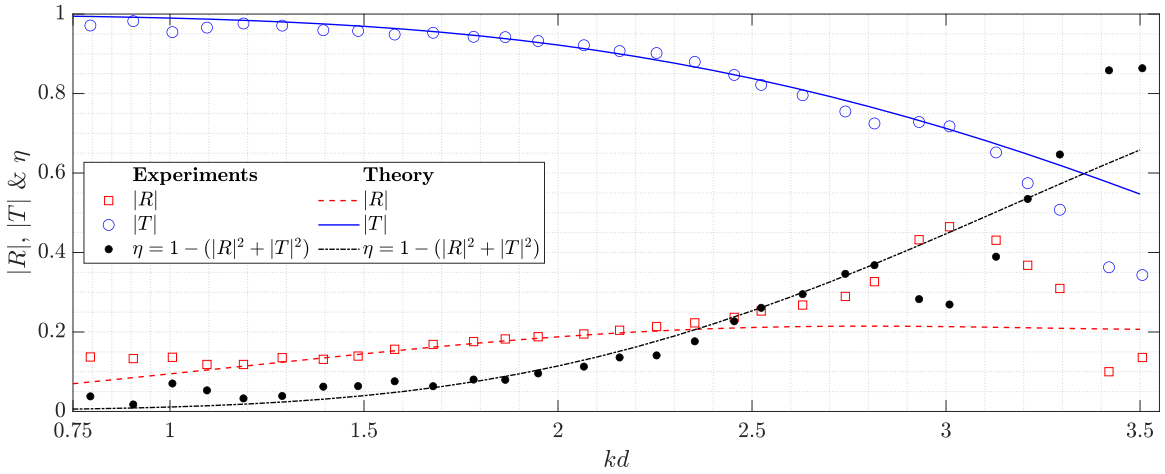

Figure 2: Comparison between experimental and theoretical values of $|R|$, $|T|$ and η.

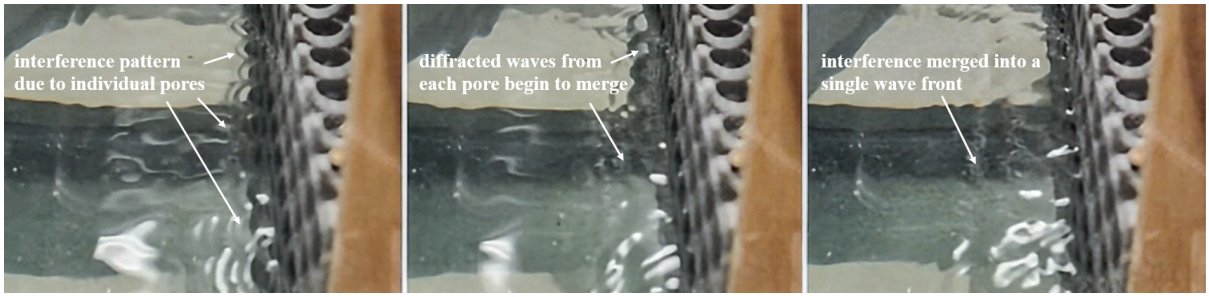

Figure 3: Interference pattern observed on the downstream water surface for $kd \approx 3.2$.

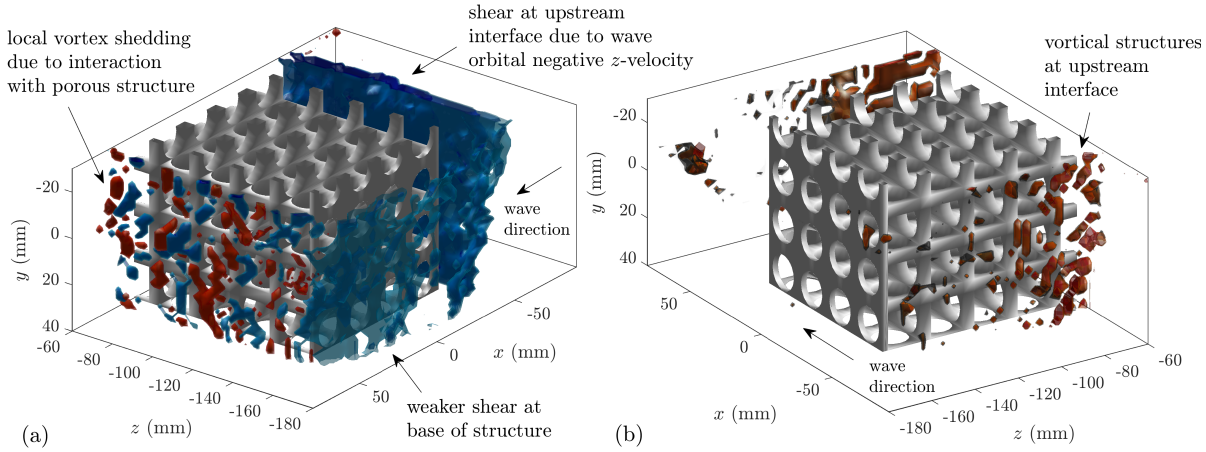

Figure 4: Instant snapshots of (a) $|\Omega_y| \geq 2$ (1/s) and (b) $Q(c_p^2/A^2) = 10^5 - 10^6$ at $kd \approx 3.2$.

To explain some of the discrepancies at higher wavenumbers, three temporal stages of the water surface during experiments at $kd \approx 3.2$ are presented in Fig. 3, revealing local interference patterns at the downstream wall. The interference pattern travels further downstream until the local pattern from each pore merges into a single wave front. Some PIV results recorded at $z \leq -60$ mm are presented in Figure 4. Isosurfaces of vorticity about the y-axis in Fig. 4(a), Ω_y, reveal alternating positive and negative vorticity at the downstream wall, and therefore clear evidence of small-scale vortex shedding. The scale of this turbulent dissipation due to the porous structure is of higher order and becomes significant at higher wavenumbers. Shear observed at the upstream interface and base is exacerbated by the non-smooth walls. The Q-criterion is non-dimensionalised by the phase velocity, c_p and wave amplitude, A, and is presented in Fig. 4(b). Vortical structures are recorded at the upstream surface due to complex interaction of wave propagation and local reflections at the solid struts. Clearly, such interactions are significant at smaller wave amplitudes and shorter wavelengths (i.e., higher kd-values), due to the comparable order of magnitude of pore dimensions and wave amplitude. Further analysis of the flow-field will be presented at the workshop, including $kd \approx 0.75$ and 2.5.

Acknowledgements: This work was supported by the Cabot Institute for the Environment Seedcorn Fund and in-kind support from LaVision UK Ltd.

References

1. E.J.G. Arcondoulis et al., 2023, Internal shear layer and vortex shedding development of a structured porous coated cylinder using tomographic particle image velocimetry, *J. Fluid Mech* **967** A17.
2. C.K. Sollitt & R.H. Cross, 1972, Wave reflection and transmission at permeable breakwaters, *MIT report No. 174.*
3. C.C. Mei, I.-C. Chan & P. L.-F. Liu, 2014, Waves of intermediate length through an array of vertical cylinders, *Env. Fluid Mech.* **14** 235–261.